Displacements, Strains and Rotations in the Central Andean Plate Boundary Zone

D. Hindle

GeoForschungsZentrum, Potsdam

J.Kley

Geologisches Institut, Universität Karlsruhe

The present day, active deformation associated with the growth of the Central Andes shown by space based geodesy reveals a consistent pattern of motion relative to stable South America nearly parallel to the direction of convergence between the Nazca and South American plates. Using balanced cross sections, we develop a geological velocity field showing how motion within the plate boundary zone varied as it migrated eastward with time. The spatial derivatives of the velocity field show the associated strains and rotations. The geological velocity field over the past ~ 10 Ma is similar in both direction and rate to that found from GPS. However, that for ~ 25 - 10 Ma is similar in direction but significantly slower. Thus it appears that the shortening rate accelerated while the convergence rate slowed. The geological velocity field also gives insight into the question of whether the Andes are undergoing gravitational collapse. The GPS data show little motion normal to the convergence direction whereas fault slip data and earthquake focal mechanisms show such motion. Analysis of the geological velocity field resolves this apparent discrepancy by showing that despite the parallel motion, extensional finite strains develop locally due to differential displacements. The geological velocity field suggests rotations broadly consistent with those determined from paleomagnetic studies. Thus differential motions within the convergence-parallel velocity field have caused the Central Andes to develop increasing curvature throughout their evolution.

INTRODUCTION

The plate boundary zone formed by subduction of the Nazca plate beneath the continental margin of South America is a spectacularly deformed, mountainous region dominated by the Andean Cordillera. Since the beginning of plate tectonic analysis of mountain belts, the Andes have been recognized as a type example of a non-collisional or Cordilleran mountain belt [*Dewey and Bird*, 1970] as opposed to the collisional type represented by the Alps and Himalaya. Their genesis remained enigmatic, with igneous processes and vertical uplift thought to have formed them [*James*, 1971] as opposed to the significant amounts of horizontal shortening and imbrication of the crust recognised in the Alps

and Himalaya [*Argand*, 1922]. It is now recognized that horizontal shortening of up to ~ 250 km in the Neogene has played the most significant part in creating their present day high-relief [*Sheffels*, 1990; *Baby et al.*, 1997; *Allmendinger et al.*, 1997; *Kley and Monaldi*, 1998; *Kley* 1999].

The Andes stretch 6000 km along strike and significant differences exist between their northern, central and southern portions [*Kley et al.*, 1999]. The central portion of the chain ($\sim 10^{\circ}$S to 25°S) is remarkable for several reasons. It contains the locus of maximum shortening ($\sim 18^{\circ}$S); the fold-thrust belts exhibit a strong curvature along strike; the Altiplano-Puna plateau dominates much of this portion of the chain (figure 1). In spite of its enormous area and an average elevation ~ 4000 m, only moderate crustal shortening is detected within the plateau. Thrusting in this portion of the Andes is localized further east in the Eastern Cordillera, a thick skinned, internal portion of the belt and the Subandean Ranges, a thin skinned, external portion. Lying west of the Altiplano-Puna is a volcanic arc and forearc region which exhibits little significant shortening (figures 1, 2 and 3). In the light of these important physiographic features, it is natural to ask what distribution and pattern of crustal deformation over their ~ 25 Ma history of formation is found in the Central Andes.

At the present day, the Andes are recognised as an actively shortening mountain belt. Space geodesy [*Lefflер et al.*, 1997; *Norabuena et al.*, 1998; *Kendrick et al.*, 2001] and earthquake focal mechanisms [*Dewey and Lamb*, 1992], give a better understanding of the deformation field that currently shapes the Central Andes. As shown in figure 2 deformation near the trench is thought to be dominated by the elastic effects of the earthquake cycle [*Norabuena et al.*, 1998; *Liu et al.* 2000, 2002], whereas that in the Eastern Cordillera and the Subandean Zone is thought to be dominated by permanent shortening.

Our goal in this paper is to present a velocity field developed from geological reconstructions and compare its predictions to those from GPS, earthquake mechanisms, fault slip indicators and paleomegnetism.

Derivation of a geological velocity field

We use a geologic velocity field (figure 4) developed by combining balanced cross sections to produce a consistent map view model of shortening *Kley* [1999]. The Andean block model (figure 3) shows large crustal blocks separated by large fault zones. At the surface, not all of the fault zones and blocks are geologically recognis-

able, since there are a multitude of small displacement, shallow structures forming the fold thrust belts. However, at depth, these structures amalgamate and transfer their displacement to large basement faults, which localise shortening into the broad zones seen in the block model (figure 5).

A variety of timing constraints including fission track [*Benjamin et. al.*, 1987; *Lamb and Hoke*, 1997; *Ege et al.*, 2001], sedimentary ages in thrust-cut parts of the foreland [e.g. *Coudert et al.*, 1996; *Jordan et al.*, 1997; *Reynolds et al.*, 2000], paleoaltimetry data [*Gregory-Wodzicki*, 2000] and paleomagnetic rotation data [*Lamb*, 2001a] also suggest that the original 25 Myr block model can be broken down into at least two distinct phases of motion giving a two stage block model (figures 3 and 4). The majority of Eastern Cordillera shortening most likely occurred $\sim$25–10 Ma. Though the EC is still active at the present day, late Neogene shortening amounts to $\leq$20 km. The Subandean ranges moved mostly $\sim$10 Ma-present. This jump of the locus of shortening of the Andes has long been speculated upon, and the balance of age data suggests it to be a real phenomenon. Formal uncertainties in timing and total shortening estimates are very difficult to assess. Data on timing may be quoted with uncertainties, but these vary according to the method being applied.

Given the volume of data now available, particularly from the Subandes, there are tight constraints on admissable cross sections. Thus, it would be difficult for the uncertainty in total shortening to be as great as 50% as suggested by *Lamb*, [2000], since this would mean that maximum shortening could be as little as 125 km across the entire chain. The tightly constrained Subandes with a wealth of available sub-surface data has $\sim$125 km shortening alone, and this estimate must be fairly rigid. We present a quantitative picture of how geological uncertainties might change shortening rate estimates in the foreland (figure 6). Values on a sample profile at 21°S are in a range 205–260 km, and timing changes may yield substantially lower geological shortening rate estimates (though the accelerating trend over time is always a feature). It is worth underlining that the Andean block mosaic (figure 1) represents the most likely case given all the geological data, and the deviations from this suggested in figure 6 are substantially less probable.

Geological displacement fields are derived for any of the block model time intervals by matching recognisable points in the deformed and retrodeformed models (figure 4). The displacement vectors (shown as velocities) are broadly parallel to slightly convergent, and

trend close to the NUVEL-1A [*DeMets et al.*, 1994] relative plate convergence vector for Nazca-South America ($\sim$079°). The fields have a constant direction of motion over time, similar to the present day GPS velocities (figure 4c). A strong gradient of shortening along strike from a central maximum (total $\sim$250 km at $\sim$18°) is present through all velocity fields, making them symmetric.

SHORTENING HISTORY

The geologic velocity fields for different time periods show an interesting phenomenon (figures 5 and 6). The velocity field for the past $\sim$10 Ma is similar in both direction and rate to that found from GPS if we ignore the coastal sites whose motion primarily reflects transient, elastic deformation associated with the seismic cycle in the trench. However, that for $\sim$25 - 10 Ma is similar in direction but significantly slower. This change is striking given that the convergence rate between the Nazca and South American plates seems to have slowed systematically over the past $\sim$25 Ma [*Pardo-Casas and Molnar*, 1987; *Somoza*, 1998; *Norabuena et al.*, 1999; *Angermann et al.*, 1999]. The observation that convergence slowed while the shortening rate accelerated implies a possible negative feedback between convergence rate and mountain building *Hindle et al.* [2002].

The geologic velocity field varies systematically with a maximum at $\sim$18° S where the Andes are the widest and diminishing to the north and south. Hence these data show the differential shortening which has been proposed by *Isacks* [1988] to be the cause of the curvature of the Andes.

CONVERGENCE-NORMAL MOTION AND LOCAL STRAINS

The geological and GPS data showing that motion within the plate boundary zone has been essentially parallel to the convergence direction preclude significant along strike motion of material within the boundary zone. This result appears inconsistent with various data suggesting motion normal to the convergence direction. Focal mechanisms in the Altiplano suggest some N-S extension [*Klosko et al.*, 2002]. Geological studies suggest that N-S extension has been a feature in the last few Myr in the high Andes [e.g. *Sebrier*, 1988; *Mercier et al.*, 1992] but was oriented E-W before the Pliocene. Other changes of stress orientations since the late Miocene have also been inferred from similar studies [*Cladouhos et al.*, 1994; *Marrett and Strecker*, 1999]. The observations of N-S extension have been

used to infer convergence normal motion perhaps due to syn-orogenic, gravitational collapse of the type observed in the Tibetan Plateau where the GPS data and focal mechanisms are consistent with geologically observed extension [*Molnar and Chen*, 1983; *Larson et al.* 1999].

Insight into the apparent discrepancy can be obtained from a geological strain field inferred from the velocity field. Using techniques from the finite element method [e.g. *Hughes*, 2000], we discretize the velocity field across a grid and write a piecewise approximation across the region [*Hindle*, 2002]. Strains are calculated over triangular elements, and represented by the lengths of the principal axes and their orientation. Regional patterns of extension can be seen from the colour coding. Finite strain axes orientations vary systematically along strike and generally mirror the topography of the Andean fold-thrust belts [*Hindle*, 2002].

Plate 1 a-c shows the total finite strain in the past ~ 25 Ma averaged over different spatial scales. Plate 1 a shows shortening at the scale of the individual (~ 100 km) triangular elements. Extension in the direction of the long axis is present in $\sim 75\%$ of the elements. This result is surprising given that the strain axes are derived from the displacement vector field which is essentially parallel to the convergence. However, this extension results from small, local differences in the magnitude of the displacement and thus does not indicate any along strike finite displacement component. To show this, we consider a larger scale, where heterogeneity is smoothed to a greater degree, giving results more related to the larger scale processes of orogenesis. Plate 1b shows less extension in the direction of the long axis at an intermediate scale. Three regions (Interandean Zone, southern Eastern Cordillera, part of northern Subandes) show contraction in all horizontal directions, another three are neutral in the long axis direction. Extension is much smaller when it occurs ($\leq 20\%$), and is present in both the northern and southern limbs of the Subandes. Strain axes orientations are also more homogeneous along strike, but still follow the trend of Andean structures. Although the regions of plate 1 b which show contraction are composed of smaller regions (plate 1 a) of dominantly along strike extension, the directions of extension are averaged. An analysis of the entire Central Andes (plate 1 c) shows that strain is contractional in all directions ($\sim$ - 17% – long axis, $\sim$ - 46% – short axis). The long axis of strain lies essentially along the NUVEL-1A convergence vector. At this mountain belt scale, contraction along strike represents movement of the ground in this direction, since the vector field is

convergent as can be seen from the vectors on the borders of the region which have a component along strike, directed towards the axis of the bend.

Comparison of the different scales shows another interesting effect. In general the strain axes are oblique to the velocity field, as previously noted for curved mountain belts [*Hindle et al.*, 2000]. However, the strain axes for the entire mountain belt (plate 1 c) are parallel and perpendicular to the velocity field.

This analysis suggests that the extension inferred from fault kinematic studies and focal mechanisms may be a local manifestation of differential shortening in the convergence direction rather than reflecting large scale motion of material. It is worth noting that fault kinematic analyses do not quantify the actual deformation absorbed due to motion on a particular set of faults because the slip magnitude and hence strain are undetermined. Similarly, the earthquake mechanisms may also reflect relatively local extension rather than the major material displacements which are shown by the GPS and geologic velocity fields.

Another way to view this issue is to recognise that the brittle upper crust deforms on discrete faults, which together cause the large scale displacement field. *Reches* [1978] showed that any 3 dimensional strain could be accomodated most efficiently on sets of up to 4 differently oriented fault planes with different slip senses. If the faults are not be sampled homogeneously, the inferred kinematic axes differ from the true strain axes. Failure to account for differences in fault slip would also cause discrepancies between the true strain and local kinematic axes. The same difficulties may result from the short time period sampled by earthquake mechanisms.

ROTATIONS

Paleomagnetic investigations have demonstrated substantial rotations of material within the Central Andes [e.g. *Butler et al.*, 1992; *Coutand et al.*, 1999; *Roperch et al.*, 2000]. Rotations vary as a function of both age of the rock - older samples showing more rotation - and position along strike of the orocline, and to a lesser degree perpendicular to the bend [*Lamb*, 2001a]. These data combined with assumed dilatation in the horizontal plane have been inverted to provide shortening estimates in the Central Andes [*Lamb*, 2001b] for the last 10 Ma which are broadly consistent with cross section balancing estimates [e.g. *Baby et al.*, 1993; *Sheffels*, 1995; *Kley and Monaldi*, 1998; *Kley*, 1999].

These rotations are consistent with those predicted by the curl of the geological velocity field, which gives the local rotation [*Lamb*, 1987; *England and Wells*,

1991]. Determining the magnitude of the rotation involves assumptions about how the upper crust deforms, in particular the orientation of faults relative to the shortening direction [*Lamb*, 2001b]. However the sign of the curl gives the expected rotation direction (clockwise - positive) at a point. Moreover, larger magnitudes should be equivalent to larger rotations. We use the discrete approximation to displacements to derive the curl at different scales as we did for strain.

At the ~ 100 km scale, rotation is heterogeneously distributed along the chain (plate 1 d), though less so than for strain (plate 1a). South of the 18° bend rotations are nearly uniformly clockwise. Around the bend anticlockwise rotation dominates. The northern limb has a mixture of clockwise and anticlockwise rotation. The largest rotations are generally at the northern and southern extremes of the study area, though there are exceptions especially on the north side of the bend. Even on the smaller scale, there is no obvious neutral zone of no rotation along the bend axis. At the intermediate scale (plate 1 e), the pattern is clearer, with the north and the bend axis showing consistently anticlockwise rotation, whilst south of the bend is clockwise. The largest scale shows effectively zero rotation, showing the vector field to be symmetrical.

IMPLICATIONS FOR THE EVOLUTION OF THE ANDES

Our analyses show the power of using a geological velocity field to represent the deformation within a plate boundary zone. The velocity field can be directly compared to both the motion between the major plates and the geodetic velocity field within the boundary zone. Spatial derivatives of the velocity field provide additional information about specific points within the velocity field. Geologic strain fields can be compared to geodetic strain fields and those calculated by summation of earthquake moment tensors [*Klosko et al.*, 2002]. Moreover, the geologic strain field gives insight into other geologic observations such as fault kinematic data. Similarly, the velocity field predicts rotations which can be compared to paleomagnetic data. Hence, combining the large scale geologic velocity field with various point measurements can yield valuable insights into boundary deformation processes.

In our view, application of this technique to the Andes gives interesting insight into the evolution of the mountain belt. The most striking aspect of the velocity field over the past 25 Ma is its parallelism to the present GPS velocity field and the plate convergence direction. The total finite strain axes (plate 1 c) are

near parallel (short axis $\sim 060^{\circ}$) or orthogonal (long axis $\sim 150^{\circ}$) to the Nazca-South America plate convergence vector. Presumably the mechanics of the plate interface constrain material in the upper plate to shorten in the convergence direction both on the short timescale of the earthquake cycle and on a longer timescale. Our analysis of long term displacements suggests that this present day pattern repeated itself with lower rates but identical direction over the last ~ 25 Ma of mountain building. *Gephart* [1994] noted the correspondence of the axes of symmetry of Andean topography and the dip of the subducted Nazca plate with the convergence vector.

Despite the parallelism of the velocity vectors, systematic along strike differences in their magnitude have produced the curved shape of the Andes. The corresponding differential shortening has caused the arc to grow symmetrically about the bend, its widest point [*Isacks*, 1988]. Hence the Andes are a Primary Arc', which develops curvature progressively due to differential shortening along strike [*Ferrill and Groshong*, 1993; *Hindle and Burkhard*, 1999]. As shown in figure 7, this differs from the original orocline idea of *Carey* [1955] in which an initially straight mountain belt is subsequently bent. Hence the paleomagnetically observed rotations reflect the continuing evolution of the arc.

Acknowledgments. We wish to thank T. Dixon, E. Norabuena and S. Stein for help in working with the SNAPP data. D.H. acknowledges financial support from Leibnizförderprogram grant no.ON70/10-1.

REFERENCES

Allmendinger, R.W., T.E. Jordan, S.M. Kay, and B.L. Isacks, The evolution of the Altiplano-Puna plateau of the Central Andes, *Annual Review of Earth and Planetary Science Letters, 25*, 139-174, 1997.

Argand, E., La tectonique de l'Asie, in *Congrès Géologique International,* pp. 171-372, Brussels, 1922.

Baby, P., B. Guillier, J. Oller, and G. Montemurro, Modèle cinématique de la Zone Subandine du coude de Santa Cruz (entre 16°S et 19°S, Bolivie) déduit de la construction de cartes équilibrées, *Comptes Rendus de l'Académie des Sciences de Paris, 317* (11), 1477-1483, 1993.

Baby, P., P. Rochat, G. Mascle, and G. Hérail, Neogene shortening contribution to crustal thickening in the back arc of the Central Andes, *Geology, 25* (10), 883-886, 1997.

Benjamin, M.T., N.M. Johnson, and C.W. Naeser, Recent rapid uplift in the Bolivian Andes: Evidence from fission-track dating, *Geology, 15,* 680-683, 1987.

Butler, R., D. Richards, T. Sempere, and L. Marshall, Paleomagnetic determinations of vertical axis tectonic rotations from Late Cretaceous and Paleocene strata of Bolivia, *Geology, 23,* 799-802, 1995.

Carey, S., The orocline concept in geotectonics, *Proceedings of the Royal Society of Tasmania, 89,* 255-288, 1955.

Cladouhos, T.T., R.W. Allmendinger, B. Coira, and E. Farrar, Late Cenozoic deformation in the Central Andes: Fault kinematics from the northern Puna, northwest Argentina and southern Bolivia, *Journal of South American Earth Sciences, 7* (2), 209-228, 1994.

Coudert, L., M. Frappa, C. Viguier, and R. Arias, Tectonic subsidence and crustal flexure in the Neogene Chaco basin of Bolivia, *Tectonophysics, 243,* 277-292, 1996.

Coutand, I., P. Roperch, A. Chauvin, P.R. Cobbold, and P. Gautier, Vertical axis rotations across the Puna plateau (northwestern Argentina) from paleomagnetic analysis of Cretaceous and Cenozoic rocks, *Journal of Geophysical Research, 104,* 22965-22984, 1999.

DeMets, C., R.G. Gordon, D.F. Argus, and S. Stein, Effect of recent revisions to the geomagnetic reversal time scale on estimates of current plate motions, *Geophysical Research Letters, 21* (20), 2191-2194, 1994.

Dewey, J.F., and J.M. Bird, Mountain Belts and the new global tectonics, *Journal of Geophysical Research, 75,* 2625-2647, 1970.

Dewey, J.F., and S.H. Lamb, Active tectonics of the Andes, *Tectonophysics, 205,* 79-95, 1992.

Ege, H., V. Jacobshagen, E. Scheuber, E. Sobel, and T. Vietor, Thrust-related exhumation revealed by apatite fission track dating, Central Andes (Southern Bolivia), *Geophysical Research Abstracts, 3,* 624, 2001.

England, P. and R. Wells, Neogene rotations and quasicontinuous deformation of the Pacific Northwest continental margin, *Geology, 19,* 978-981. 1991

Ferrill, D.A., and R.H. Groshong, Kinematic model for the curvature of the northern Subalpine Chain, France, *Journal of Structural Geology, 15* (3-5), 523-541, 1993.

Gephart, J., Topography and subduction geometry in the cnetral Andes: Clues to the mechanics of a noncollisional orogen, *Journal of Geophysical Research, 99,* B6, 12279-12288, 1994.

Gregory-Wodzicki, K., Uplift history of the Central and Northern Andes: A review, *Bulletin of the Geological Society of America, 112,* 1091-1105, 2000.

Hindle, D., Finite strain variations along strike of mountain belts, in *New insights into structural modelling and interpretation,* edited by D. Nieuwland, Special Publications of the Geological Society of London, 2002.

Hindle, D., and M. Burkhard, Strain, displacement and rotation associated with the formation of curvature in fold belts; the example of the Jura arc, *Journal of Structural Geology, 21,* 1089-1101, 1999.

Hindle, D., J. Kley, E. Klosko, S. Stein, T. Dixon and E. Norabuena, Consistency of geologic and geodetic displacements during Andean orogenesis, *Geophysical Research Letters, in press,* 2002.

Hughes, T. *The Finite Element Method. Linear static and dynamic finite element analysis,* 676 pp., Dover, 2000

James, D.E. Plate Tectonic Model for the Evolution of the Central Andes, *Geological Society of America Bulletin, 82,* 3325-3346, 1971.

Jordan, T.E., J.H. Reynolds, and J.P. Erikson, Variability in age of initial shortening and uplift in the Central Andes, 16-33°30′S, in *Tectonic uplift and climate change,* edited by W.F. Ruddiman, pp.41-61, Plenum, New York, 1997.

Kendrick, E., M. Bevis, R. Smalley, B. Brooks, An integrated crustal velocity field for the central Andes, *Geo-*

chemistry Geophysics Geosystems, 2, paper no. 2001GC00-0191, 2001.

Kley, J., Geologic and geometric constraints on a kinematic model of the Bolivian orocline, *Journal of South American Earth Sciences, 12,* 221-235, 1999.

Kley, J., and C.R. Monaldi, Tectonic shortening and crustal thickness in the Central Andes: How good is the correlation?, *Geology, 26* (8), 723-726, 1998.

Kley, J., C.R. Monaldi, and J.A. Salfity, Along-strike segmentation of the Andean foreland: causes and consequences, *Tectonophysics, 301,* 75-94, 1999.

Klosko, E. R., S. Stein, J. Kley, D. Hindle, T. Dixon, E. Norabuena, M. Liu Comparison of geodetic, geologic, and seismological observations of Andean mountain building, in *Plate Boundary Zones,* edited by S. Stein and J. Freymueller, *this volume*, AGU, Washington, D. C., 2002.

Lamb, S., Active deformation of the Bolivian Andes, South America, *Journal of Geophysical Research, 105,* 25627-25653, 2000.

Lamb, S., Vertical axis rotation in the Bolivian orocline, South America 1. Paleomagnetic analysis of Cretaceous and Cenozoic rocks, *Journal of Geophysical Research, 106* (B11), 26605-26632, 2001a.

Lamb, S., Vertical axis rotation in the Bolivian orocline, South America 2. Kinematic and dynamical implications, *Journal of Geophysical Research, 106* (B11), 26633-26653, 2001b.

Lamb, S., and L.Hoke, Origin of the high plateau in the Central Andes, Bolivia, South America, *Tectonics, 16,* 623-649, 1997.

Larson, K., R. Burgmann, R. Bilham, and J. T. Freymueller, Kinematics of the India-Eurasia collision zone from GPS measurements, *Journal of Geophysical Research, 104,* 1077-1094, 1999.

Leffler, L., S. Stein, A. Mao, T. Dixon, M.A. Ellis, L. Ocola, and I.S. Sacks, Constraints on present day shortening rate across the central eastern Andes from GPS data, *Geophysical Research Letters, 24* (9), 1031-1034, 1997.

Liu, M., Y. Zhu, S. Stein, Y. Yang, and J. Engeln, Crustal shortening in the Andes: Why do GPS rates differ from geological rates, *Geophysical Research Letters 18,* 3005-3008, 2000.

Liu, M., Y. Yang, S. Stein, and E. Klosko, Crustal shortening and extension in the Andes from a viscoelastic model, in *Plate Boundary Zones* edited by S. Stein and J. Freymueller, *this volume,* AGU, Washington, D. C.,2002.

Marrett, R., and M.R. Strecker, Response of intracontinental deformation in the central Andes to late Cenozoic reorganization of South American Plate motions, *Tectonics, 19* (3), 452-467, 2000.

Mercier, J., M. Sebrier, A. Lavenu, J. Cabrera, O. Bellier, J.-F. Dumont, and J. Machare, Changes in the tectonic regime above a subduction zone of Andean type: The Andes of Peru and Bolivia during the Pliocene-Pleistocene, *Journal of Geophysical Research, 97* (B8), 11945-11982, 1992.

Molnar, P., and W.-P. Chen, Focal depths and fault plane solutions of earthquakes under the Tibetan plateau, *Journal of Geophysical Research, 88,* 1180-1196 1983.

Norabuena, E., L. Leffler-Griffin, A. Mao, T. Dixon, S. Stein, I.S. Sacks, L. Ocala, and M. Ellis, Space geodetic observations of Nazca-South America convergence along the

Central Andes, *Science, 279,* 358-362, 1998.

Reches, Z., Analysis of faulting in a three-dimensional strain field, *Tectonophysics, 47,* 109-129, 1978.

Reynolds, J.H., C.I. Galli, R.M. Hernández, B.D. Idleman, J.M. Kotulla, R.V. Hilliard, and C.W. Naeser, Middle Miocene tectonic development of the transition zone, Salta Province, northwestern Argentina: Magnetic stratigraphy from the Metán Subgroup, Sierra de González, *Bulletin of the Geological Society of America, 112,* 1736-1751, 2000

Roperch, P., M. Fornari, G. Hérail, and G.V. Parraguez, Tectonic rotations within the Bolivian Altiplano: Implications for the geodynamic evolution of the central Andes during the late Tertiary, *Journal of Geophysical Research, 105* (B1), 795-820, 2000.

Sébrier, M., A. Lavenu, M. Fornari, and J-P. Soulas, Tectonics and uplift in Central Andes (Peru, Bolivia and Northern Chile) from Eocene to present, *Géodynamique 3* (1-2), 85-106

Sheffels, B., Is the bend in the Bolivian Andes an Orocline?, in *Petroleum Basins of South America,* edited by A.J. Tankard, R. Suárez S., and H.J. Welsink, pp. 511-522, Tulsa, 1995.

Sheffels, B.M., Lower bound on the amount of crustal shortening in the central Bolivian Andes, *Geology, 18,* 812-815, 1990.

D. Hindle, GeoForschungsZentrum, Telegrafenberg C2, D-14473, Potsdam, Germany (e-mail: hindle@gfz-potsdam.de)

J. Kley, Geologisches Institut, Universität Karlsruhe, PO Box 6980, D-76128, Karlsruhe, Germany (e-mail: jonas.kley@bio-geo.uni-karlsruhe.de)

Figure 1. The Nazca-South America plate boundary zone in the region of the Central Andes. NUVEL1A relative plate convergence vector for Nazca-SA is projected. The upper plate (South America) margin is dominated by the high relief (4–6000m) Andean Cordillera. This is divided into several major geological provinces (forearc, volcanic arc, Altiplano-Puna plateau, Eastern Cordillera and Subandes). Position of detailed cross section (figure 5) is shown by black line in foreland.

Figure 1. The Nazca-South America plate boundary zone in the region of the Central Andes. NUVEL1A relative plate convergence vector for Nazca-SA is projected. The upper plate (South America) margin is dominated by the high relief (4–6000m) Andean Cordillera. This is divided into several major geological provinces (forearc, volcanic arc, Altiplano-Puna plateau, Eastern Cordillera and Subandes). Position of detailed cross section (figure 5) is shown by black line in foreland.

Figure 2. Sketch cross section across the Andean plate boundary zone. The active deformation of the Andes is strongly related to the behaviour of the plate interface, estimated to be locked $\sim 50\%$ [*Norabuena et al.*, 1998]. Motion transferred to the upper plate is stored elastically in the forearc, but deforms the eastern foreland plastically and permanently. Thus the velocity gradient across the zone shows permanent shortening in the east, whilst in the west it shows elastic and recoverable deformation.

Figure 2. Sketch cross section across the Andean plate boundary zone. The active deformation of the Andes is strongly related to the behaviour of the plate interface, estimated to be locked $\sim 50\%$ [*Norabuena et al.*, 1998]. Motion transferred to the upper plate is stored elastically in the forearc, but deforms the eastern foreland plastically and permanently. Thus the velocity gradient across the zone shows permanent shortening in the east, whilst in the west it shows elastic and recoverable deformation.

Figure 3. Andean plate boundary zone retro-deformed, by decomposing it into large crustal blocks (see figure 5). (a) 25Ma, most of Andean shortening pulled out of the margin, restores motion in both the Eastern Cordillera (EC) and Subandean Zone. (b) Intermediate stage of restoration at ~ 10Ma, with Eastern Cordillera shortening largely accomplished, and only the Subandean shortening retro-deformed. (c) Present day, showing crustal block boundaries and postions of major units, EC - Eastern Cordillera, IA - Inter Andean Zone.

Figure 3. Andean plate boundary zone retro-deformed, by decomposing it into large crustal blocks (see figure 5). (a) 25Ma, most of Andean shortening pulled out of the margin, restores motion in both the Eastern Cordillera (EC) and Subandean Zone. (b) Intermediate stage of restoration at ~ 10Ma, with Eastern Cordillera shortening largely accomplished, and only the Subandean shortening retro-deformed. (c) Present day, showing crustal block boundaries and postions of major units, EC - Eastern Cordillera, IA - Inter Andean Zone.

Figure 4. Time averaged velocity vectors from the block model (figure 2). (a) Motion confined to the Eastern Cordillera, at $\sim$ 5–8 mmyr^{-1}. (b) Motion confined mostly to Subandes at $\sim$8-14 mmyr^{-1}. (c) GPS data from the SNAPP experiment [*Norabuena et al.*, 1998] - modified from *Hindle et al.* [2002]. Dashed vectors represent points undegoing transient, elastic loading related to the earthquake cycle and therefore not directly comparable to geologic shortening. (d) Motion averaged over 25 Ma. (e) The shortening gradient along strike 25 - 10 Ma and 10 - 0 Ma with bars showing coastal (hence maximum) velocity magnitudes at different latitudes.

Figure 4. Time averaged velocity vectors from the block model (figure 2). (a) Motion confined to the Eastern Cordillera, at $\sim$ 5–8 mmyr^{-1}. (b) Motion confined mostly to Subandes at $\sim$8-14 mmyr^{-1}. (c) GPS data from the SNAPP experiment [*Norabuena et al.*, 1998] - modified from *Hindle et al.* [2002]. Dashed vectors represent points undegoing transient, elastic loading related to the earthquake cycle and therefore not directly comparable to geologic shortening. (d) Motion averaged over 25 Ma. (e) The shortening gradient along strike 25 - 10 Ma and 10 - 0 Ma with bars showing coastal (hence maximum) velocity magnitudes at different latitudes.

Figure 5. The relationship between block models and balanced cross sections. The geologcial cross section (a) is restored (b) to obtain the magnitudes of shortening accomodated by high level structures. Basement structures are adjusted to fit the shortening magnitudes and depths to detachment. (c) The deformed cross section is stripped of the folded and faulted cover rocks and simplified to a stack of overlapping basement blocks. Serial simplified cross sections are used to build the deformed block model. (d) The basement blocks of the example section restored to their original positions separated by their relative displacements. Although not a basement thrust, the thrust front is marked as a narrow gap to obtain the correct width of the deforming area.

Figure 5. The relationship between block models and balanced cross sections. The geologcial cross section (a) is restored (b) to obtain the magnitudes of shortening accomodated by high level structures. Basement structures are adjusted to fit the shortening magnitudes and depths to detachment. (c) The deformed cross section is stripped of the folded and faulted cover rocks and simplified to a stack of overlapping basement blocks. Serial simplified cross sections are used to build the deformed block model. (d) The basement blocks of the example section restored to their original positions separated by their relative displacements. Although not a basement thrust, the thrust front is marked as a narrow gap to obtain the correct width of the deforming area.

Figure 6. Uncertainties in geological shortening and timing estimates through time ($\sim$ 40 Ma). The lowermost graphs represent summed strain rate estimates for different thrust belt segments along a transect at 21° S. The uncertainties in total shortening mostly arise from poorly constrained Neogene shortening values in the polyphase deformed internal parts of the thrust belt. Uncertainties in timing are due to scarce stratigraphic control in the thick continental foredeep fill and to the preliminary nature of thermochronologic data bearing on the timing of exhumation. Uppermost graph shows the variation of convergence rates over the same time period.

Figure 6. Uncertainties in geological shortening and timing estimates through time ($\sim$ 40 Ma). The lowermost graphs represent summed strain rate estimates for different thrust belt segments along a transect at 21° S. The uncertainties in total shortening mostly arise from poorly constrained Neogene shortening values in the polyphase deformed internal parts of the thrust belt. Uncertainties in timing are due to scarce stratigraphic control in the thick continental foredeep fill and to the preliminary nature of thermochronologic data bearing on the timing of exhumation. Uppermost graph shows the variation of convergence rates over the same time period.

Figure 7. Different kinematics of curved mountain belts. (a) The Primary Arc which undergoes a progressive evolution of curvature due to differential, parallel motion of material along strike of the belt - shown by the single stage of displacement vectors. (b) The orocline which forms as an initially straight chain and then undergoes secondary bending - shown as two stages of displacement vectors.

Figure 7. Different kinematics of curved mountain belts. (a) The Primary Arc which undergoes a progressive evolution of curvature due to differential, parallel motion of material along strike of the belt - shown by the single stage of displacement vectors. (b) The orocline which forms as an initially straight chain and then undergoes secondary bending - shown as two stages of displacement vectors.

Plate 1. Total finite strain and rotation for Andean shortening at three different scales: a-c - strain axes orientations (black crosses) with colours showing degree of extension (positive) or contraction (negative) in the direction of the long axes; d-f - curl of the displacement function with colours showing rotation (rates) - clockwise (positive). (a) Strain of individual triangular elements (~ 100 km scale) (b) amalgamated strains of regions corresponding roughly to major structural units of the foreland from figure 1c (~ 300 km scale) (c) total strain tensor for the Central Andes (~ 3000 km scale). Also shown is the relative orientation of the GPS/NUVEL-1A convergence vectors and the axes of the total strain ellipse. (d) rotation (curl) ~ 100 km scale, (b) rotation (curl) ~ 300 km scale (c) rotation (curl) ~ 3000 km scale

Plate 1. Total finite strain and rotation for Andean shortening at three different scales: a-c - strain axes orientations (black crosses) with colours showing degree of extension (positive) or contraction (negative) in the direction of the long axes; d-f - curl of the displacement function with colours showing rotation (rates) - clockwise (positive). (a) Strain of individual triangular elements (~ 100 km scale) (b) amalgamated strains of regions corresponding roughly to major structural units of the foreland from figure 1c (~ 300 km scale) (c) total strain tensor for the Central Andes (~ 3000 km scale). Also shown is the relative orientation of the GPS/NUVEL-1A convergence vectors and the axes of the total strain ellipse. (d) rotation (curl) ~ 100 km scale, (b) rotation (curl) ~ 300 km scale (c) rotation (curl) ~ 3000 km scale

CONSISTENT DEFORMATION ANDES

HINDLE, KLEY

CONSISTENT DEFORMATION ANDES

HINDLE, KLEY

CONSISTENT DEFORMATION ANDES

HINDLE, KLEY

CONSISTENT DEFORMATION ANDES

HINDLE, KLEY

CONSISTENT DEFORMATION ANDES

HINDLE, KLEY

CONSISTENT DEFORMATION ANDES

HINDLE, KLEY

CONSISTENT DEFORMATION ANDES

HINDLE, KLEY

CONSISTENT DEFORMATION ANDES

HINDLE, KLEY

CONSISTENT DEFORMATION ANDES

HINDLE, KLEY

CONSISTENT DEFORMATION ANDES

HINDLE, KLEY

CONSISTENT DEFORMATION ANDES

HINDLE, KLEY

CONSISTENT DEFORMATION ANDES

HINDLE, KLEY

CONSISTENT DEFORMATION ANDES

HINDLE, KLEY

CONSISTENT DEFORMATION ANDES

HINDLE, KLEY

Figure 1

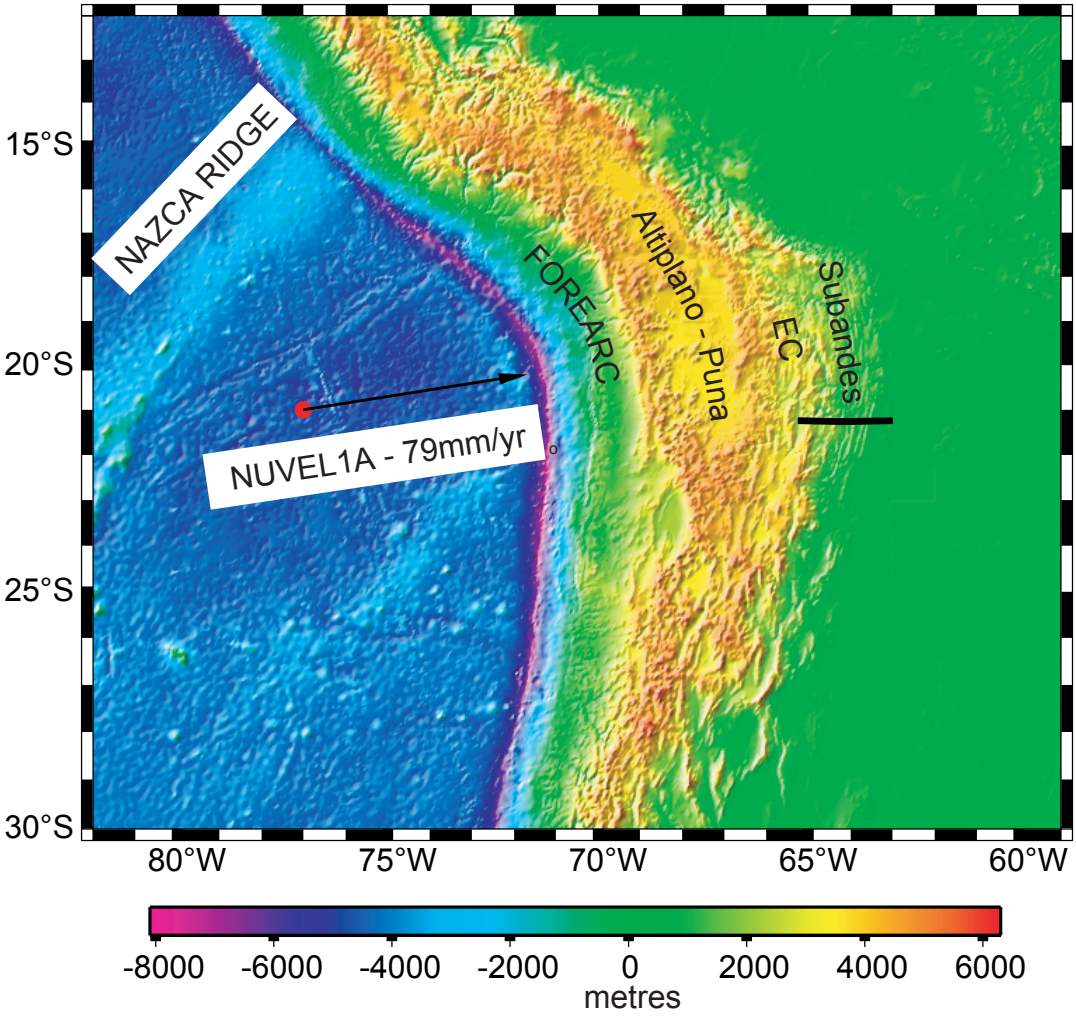
NAZCA RIDGE
FOREARC
Altiplano - Puna
EC
Subandes
NUVEL1A - 79mm/yr
15°S
20°S
25°S
30°S
80°W
75°W
70°W
65°W
60°W
-8000
-6000
-4000
-2000
0
2000
4000
6000
metres

Figure 2

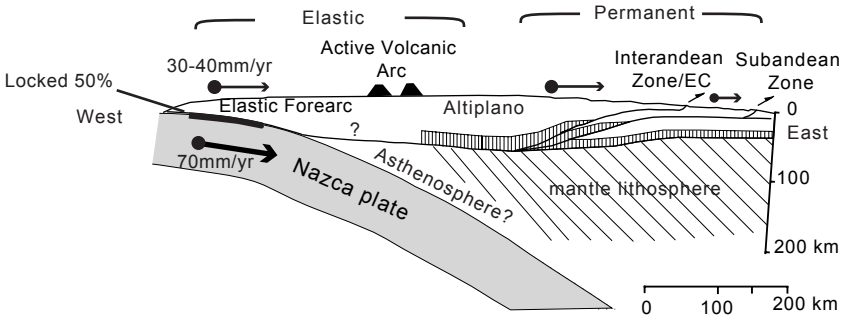
Elastic
Permanent
Active Volcanic
Arc
30-40mm/yr
Locked 50%
West
Elastic Forearc
?
Altiplano
Interandean
Zone/EC
Subandean
Zone
0
East
100
200 km
70mm/yr
Nazca plate
Asthenosphere?
mantle lithosphere
0
100
200 km

Figure 3

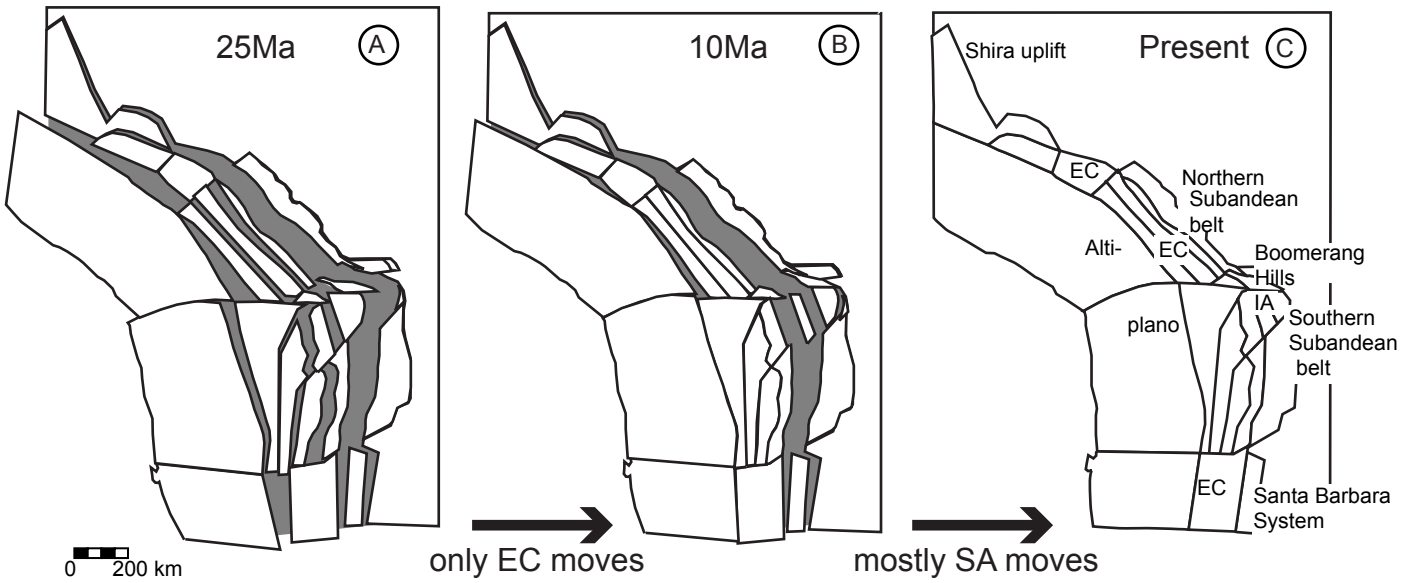
25Ma
A
10Ma
B
Shira uplift
Present
C
EC
Northern
Subandean
belt
Alti-
plano
EC
Boomerang
Hills
IA
Southern
Subandean
belt
EC
Santa Barbara
System
0
200 km
only EC moves
mostly SA moves

Figure 4

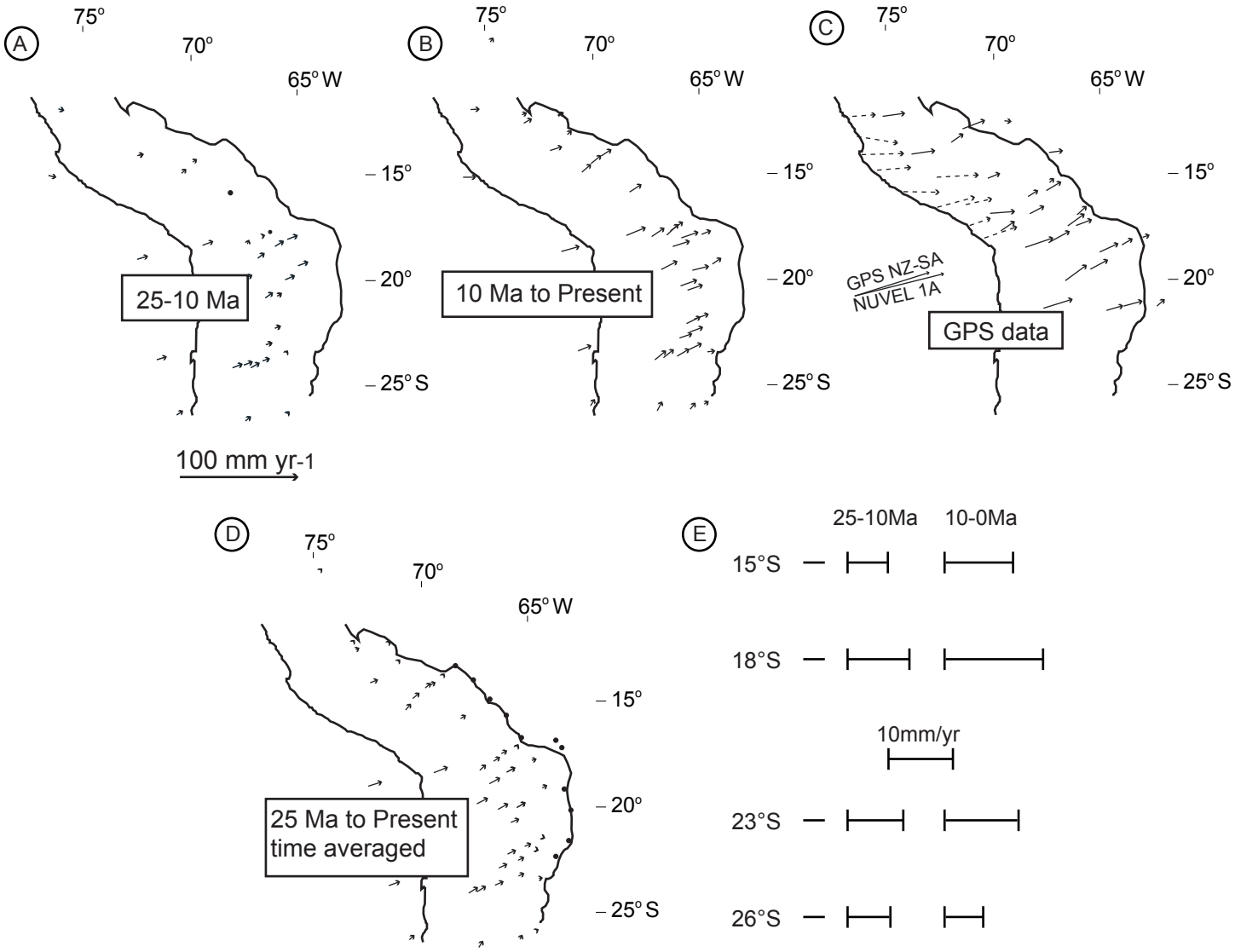
A
75°
70°
65° W
15°
20°
25° S
25-10 Ma
100 mm yr-1
B
10 Ma to Present
C
GPS NZ-SA
NUVEL 1A
GPS data
D
25 Ma to Present
time averaged
E
25-10Ma
10-0Ma
15°S
18°S
10mm/yr
23°S
26°S

Figure 5

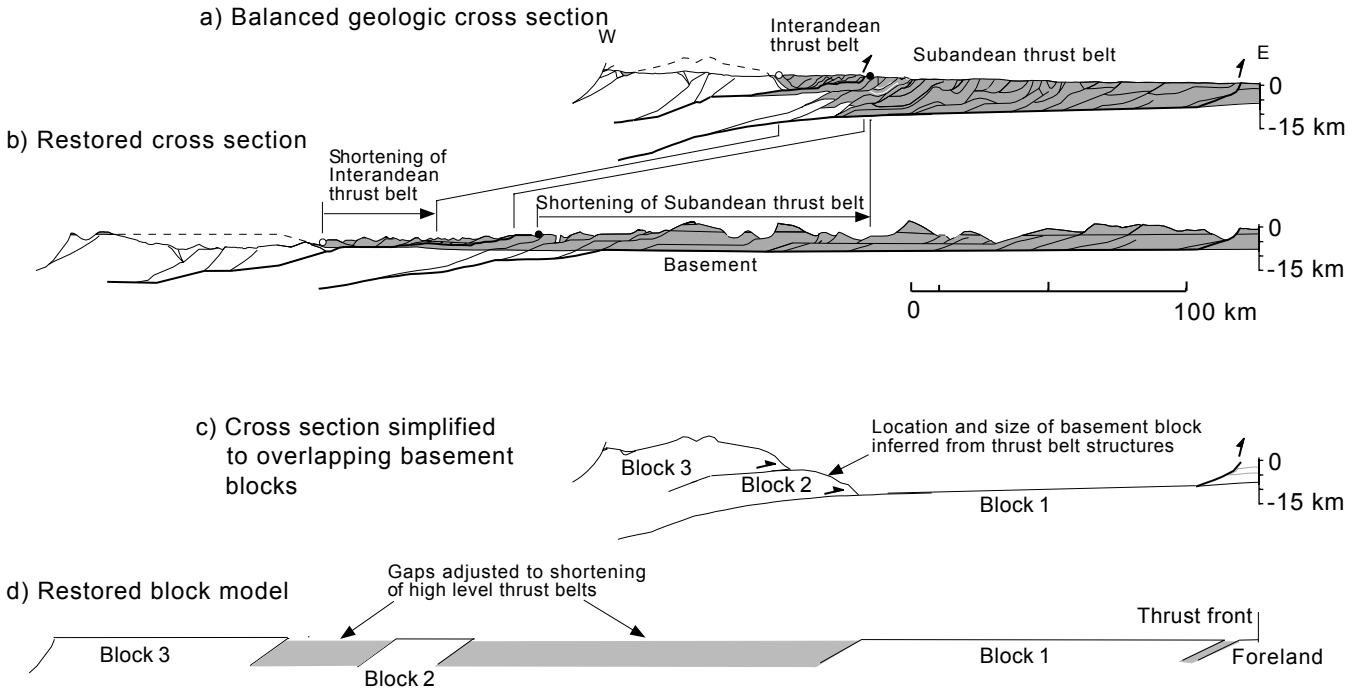
a) Balanced geologic cross section
W
Interandean thrust belt
Subandean thrust belt
E
0
-15 km
b) Restored cross section
Shortening of Interandean thrust belt
Shortening of Subandean thrust belt
0
-15 km
Basement
0
100 km
c) Cross section simplified to overlapping basement blocks
Location and size of basement block inferred from thrust belt structures
Block 3
Block 2
Block 1
0
-15 km
d) Restored block model
Gaps adjusted to shortening of high level thrust belts
Thrust front
Block 3
Block 2
Block 1
Foreland

Figure 6

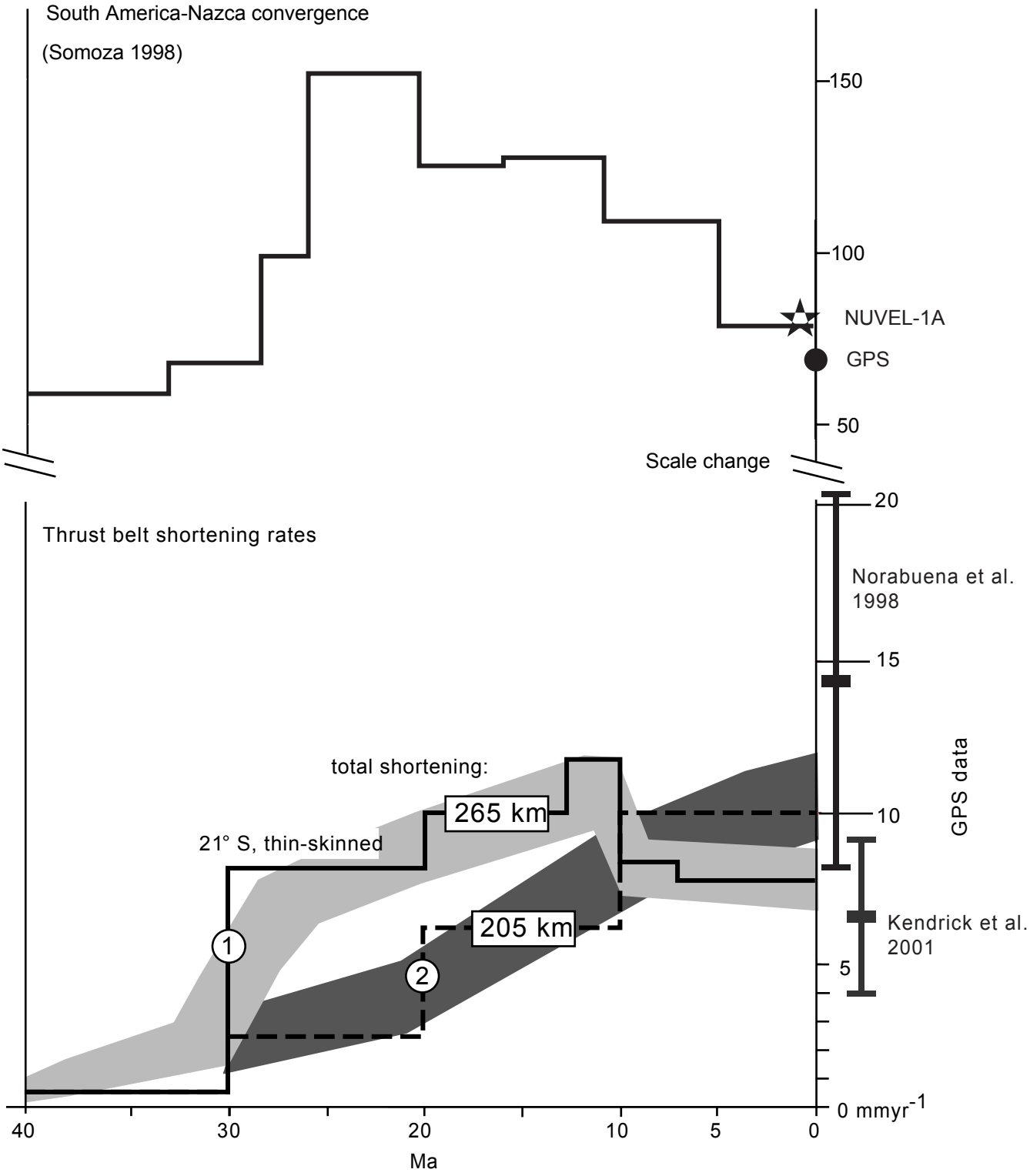

(1) Strongly shortened Eastern Cordillera, 13 Ma onset of Subandean thrusting

(2) Weakly shortened Eastern Cordillera, 10 Ma onset of Subandean thrusting

Plate 1

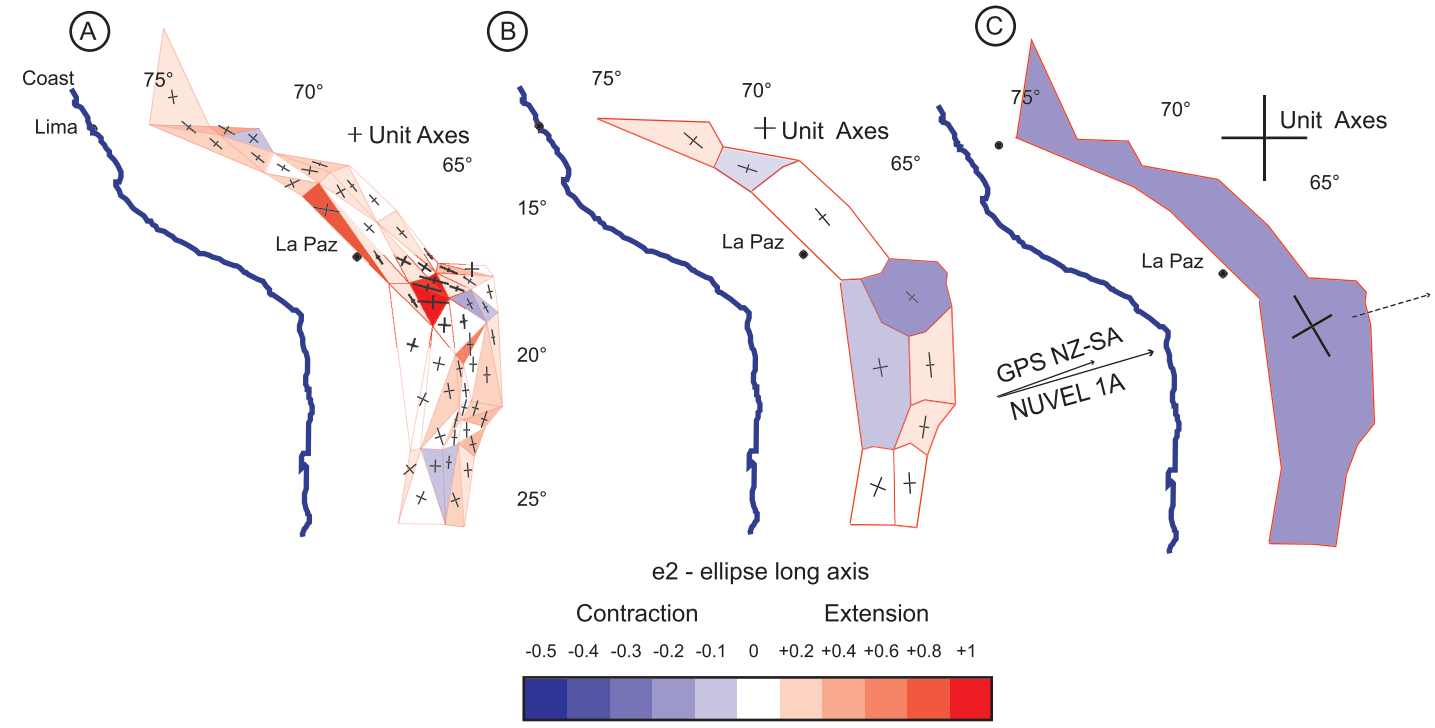

e2 - ellipse long axis

Contraction Extension

-0.5 -0.4 -0.3 -0.2 -0.1 0 +0.2 +0.4 +0.6 +0.8 +1

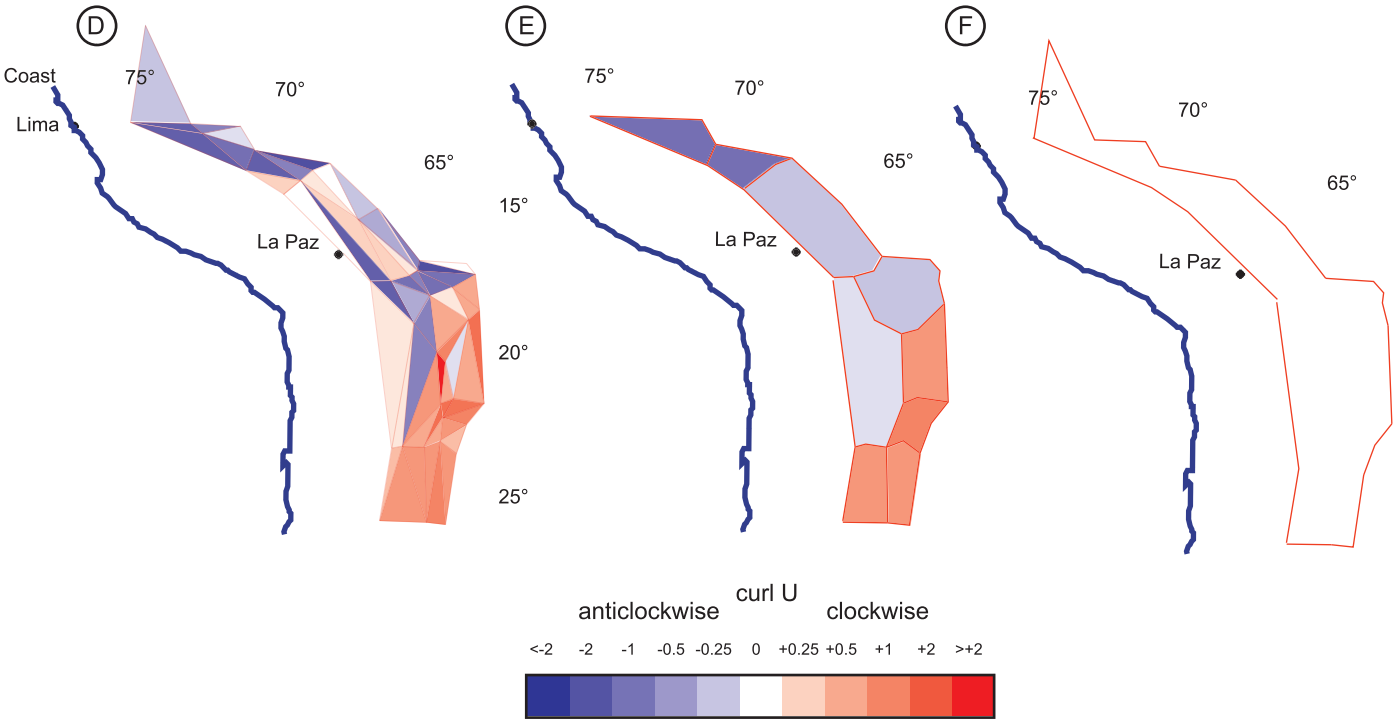

curl U

anticlockwise clockwise

<-2 -2 -1 -0.5 -0.25 0 +0.25 +0.5 +1 +2 >+2

figure 7

A) Primary arc - continuous evolution of curvature

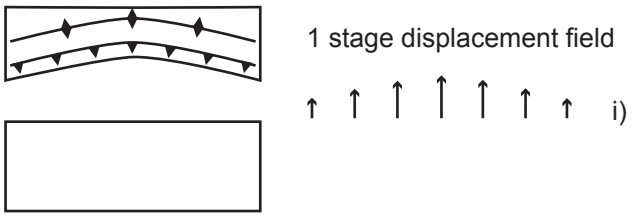

B) Orcoline (secondary bending)